Proceeding Paper

Aptamer-Based Biosensor Design for Simultaneous Detection of Cervical Cancer-Related MicroRNAs [†]

Radu Tamaian

ICSI Analytics, National Institute for Research and Development for Cryogenic and Isotopic Technologies—ICSI Rm. Vâlcea, 4th Uzinei Street, Râmnicu Vâlcea, VL, Romania; radu.tamaian@icsi.ro

† Presented at the 10th International Electronic Conference on Sensors and Applications (ECSA-10), 15–30 November 2023; Available online: https://ecsa-10.sciforum.net/.

Abstract: This study presents the design of an innovative aptamer-based biosensor for the detection of circulating microRNAs (miRNAs) associated with cervical cancer development. The selected panel includes circulating miRNAs known to play vital roles in cervical cancer pathogenesis, regulating processes such as cellular proliferation, migration, invasion, angiogenesis, apoptosis, inflammatory responses, and metastasis. The biosensor's design can be optimized to ensure high sensitivity, low limits of detection, and robust performance in clinical settings. This novel biosensor design holds great promise for facilitating non-invasive detection and personalized therapeutic approaches for cervical cancer patients.

Keywords: aptamer; biosensor; cervical cancer; circulating microRNAs

1. Introduction

Cervical cancer is a significant global health burden with a high prevalence in many regions [1], being the fourth most common cancer among women and accounting for 90% of new cases and fatalities in low- and middle-income countries [2]. To address this challenge, there is an urgent need for innovative diagnostic tools that can enable early detection and personalized therapeutic interventions. One such promising approach involves the design and development of aptamer-based biosensors (aptasensors) [3,4]. Aptamers are single-stranded DNA or RNA molecules that can bind specifically to target molecules with high affinity. They are often referred to as "chemical antibodies" due to their ability to recognize and bind to specific targets, including biomarkers associated with various diseases, such as cancer [5].

This paper refers to a design study for the further development of an aptasensor for the detection of circulating microRNAs (miRNAs) associated with cervical cancer development. In the context of cancer, including cervical cancer, altered expression levels of specific miRNAs have been identified in the bloodstream, known as circulating miRNAs. These circulating miRNAs can serve as potential biomarkers for early cancer detection and monitoring disease progression [6,7].

Aptasensors offer several advantages over traditional diagnostic methods. They are highly specific and sensitive, allowing for the detection of very small quantities of target molecules in complex biological samples. Aptasensors can be engineered to detect multiple miRNA targets simultaneously, providing a comprehensive profile of miRNA expression patterns associated with cervical cancer. Aptasensors offer a non-invasive and cost-effective diagnostic approach. Blood samples, which are easy to obtain, can be used for miRNA detection. Aptasensors, when used in place of more intrusive procedures such as biopsies, reduce patient discomfort and the risk of complications.

2. Materials and Methods

An extended panel of circulating miRNAs known to play crucial roles in the pathogenesis of cervical cancer (regulating processes such as cellular proliferation, migration, invasion, angiogenesis, apoptosis, inflammatory responses, and metastasis) [8] was chosen for the design of the aptasensor.

The RNA sequences of the circulating miRNAs were extracted from the *RNAcentral database* (v22) [9].

All the aptamer sequences corresponding to the circulating miRNA panel were predicted with the help of the web-based software tool *NHLBI-AbDesigner* [10]. The best-ranked sequences were selected with the help of the Immunogenicity Score. Immunogenicity Score is calculated based on a hydropathy scale (range: −4.5 to 4.5), and helps assess the likelihood that the chosen peptide sequence will be specifically recognized.

The *RNA Folding Form* from the *mfold* web server [11] was used for modeling, displaying, and analyzing the secondary structure of designed aptamers. The preset folding temperature of software is fixed at 37°; meanwhile, the ionic conditions were set to 1.0 M NaCl and no divalent ions. The Gibbs free energy (ΔG) was utilized to predict the stability of RNA aptamer secondary structures. In this context, a positive value for ΔG means that the folding process is not spontaneous and requires an input of energy. This could be due to an unfavorable change in enthalpy (ΔH) or a decrease in entropy (ΔS) that is not compensated by a favorable change in enthalpy. In other words, the RNA molecule is more stable in its unfolded state than in its folded state under these conditions [12].

3. Results and Discussion

The Immunogenicity Score ranking of *NHLBI-AbDesigner* was used to select the most immunogenic aptamers (RNA sequence), while the *RNA Folding Form* was used to predict the most stable RNA aptamer secondary structures (Table 1).

Table 1. The best-ranked predicted aptamer sequences (Immunogenicity Score rank = 1) and the corresponding ΔG of their secondary structures.

miRNA	Aptamer (Predicted) Sequence [N_1-N_n]	Aptamer Folding—Secondary Structure (ΔG in kcal/mol)
miR-10b	CGAUUCUAGGGGAAU [8–22]	3xST: −0.5/−0.2/0.4
	UCGAUUCUAGGGGAA [7–21]	3xST: 0.4/0.7/1.0
miR-15b-3p	CAUUAUUUGCUGCUC [6–20]	2xST: 2.0/2.8
miR-15b-5p	AGCAGCACAUCAUGG [2–16]	2xST: 0.9/1.9
miR-17-3p[PC]	CUGCAGUGAAGGCAC [2–16]	2xST: −1.1/−0.2
miR-17-5p[PC]	GCUUACAGUGCAGGU [7–21]	−1.2
	UGCUUACAGUGCAGG [6–20]	−1.9
	GUGCUUACAGUGCAG [5–19]	4xST: −2.7/−2.5/−2.5/−2.1
miR-21[BC]	CAGACUGAUGUUGAC [9–23]	−0.4
miR-27b-3p	GUGGCUAAGUUCUGC [7–21]	3xST: 0.2/1.0/1.1
miR-27b-5p	AGCUGAUUGGUGAAC [8–22]	−0.2
miR-32-3p	AGUGUGUGUGAUAUU [7–21]	1.0
	UAGUGUGUGUGAUAU [6–20]	1.3
	UUAGUGUGUGUGAUA [5–19]	3xST: 2.80/3.3/3.3
	AUUUAGUGUGUGUGA [3–17]	6xST: 3.2/3.5/3.7/4.0/4.1/4.2
	AAUUUAGUGUGUGUG [2–16]	3xST: 2.9/3.2/3.7
miR-32-5p	CAUUACUAAGUUGCA [8–22]	3xST: 2.8/3.2/3.7
	ACAUUACUAAGUUGC [7–21]	3xST: 2.3/2.3/3.2
	CACAUUACUAAGUUG [6–20]	2xST: 2.0/2.7
	GCACAUUACUAAGUU [5–19]	2xST: 2.0/2.9

	UGCACAUUACUAAGU [4–18]	2xST: 2.1/2.8
	UUGCACAUUACUAAG [3–17]	2xST: 3.2/4.2
miR-124-3p[PC]	GGCACGCGGUGAAUG [4–18]	2xST: 0.1/1.1
miR-124-5p[PC]	GUGUUCACAGCGGAC [2–16]	−0.9
	CGUGUUCACAGCGGA [1–15]	2xST: −1.1/−0.5
miR-130a-3p	GCAAUGUUAAAAGGG [5–19]	4xST: 3.6/4.1/4.5/4.5
miR-130a-5p	UCACAUUGUGCUACU [8–22]	0.9
	UUCACAUUGUGCUAC [7–21]	0.9
miR-138-1-3p	CACAACACCAGGGCC [8–22]	No folding is possible
miR-138-2-3p	CACGACACCAGGGUU [8–22]	2xST: 0.6/0.7
	UCACGACACCAGGGU [7–21]	0.7
	UUCACGACACCAGGG [6–20]	4xST: 2.9/3.4/3.7/3.9
miR-138-5p	GUGUUGUGAAUCAGG [6–20]	2xST: 0.9/1.5
	GGUGUUGUGAAUCAG [5–19]	−0.1
	AGCUGGUGUUGUGAA [1–15]	2xST: 0.3/0.9
miR-143-3p[PC]	GAUGAAGCACUGUAG [4–18]	5xST: 2.7/2.9/3.2/3.3/3.7
	GAGAUGAAGCACUGU [2–16]	2xST: 1.8/2.5
	UGAGAUGAAGCACUG [1–15]	3xST: 1.8/2.2/2.5
miR-143-5p[PC]	GGUGCAGUGCUGCAU [1–15]	−4.5
miR-146a	ACUGAAUUCCAUGGG [7–21]	5xST: 1.3/1.5/1.8/1.8/2.5
miR-192-3p	UUCCAUAGGUCACAG [8–22]	1.7
	GCCAAUUCCAUAGGU [3–17]	−0.4
	UGCCAAUUCCAUAGG [2–16]	2xST: 1.4/2.3
miR-192-5p	UAUGAAUUGACAGCC [7–21]	1.6
	CUAUGAAUUGACAGC [6–20]	1.6
	CCUAUGAAUUGACAG [5–19]	1.6
	GACCUAUGAAUUGAC [3–17]	2xST: 3.1/4.0
miR-214	GGCACAGACAGGCAG [7–21]	−0.9
	GCAGGCACAGACAGG [4–18]	No folding is possible
miR-218-1-3p	CGUCAAGCACCAUGG [8–22]	7xST: 1.4/1.4/1.7/2.1/2.2/2.3/2.3
miR-218-2-3p	CUGUCAAGCACCGCG [8–22]	3xST: 0.4/1.2/1.3
miR-218-5p	GUGCUUGAUCUAACC [3–17]	2.1
miR-328-3p	GGCCCUCUCUGCCCU [3–17]	−2.4
	UGGCCCUCUCUGCCC [2–16]	−2.4
	CUGGCCCUCUCUGCC [1–15]	−1.6
miR-328-5p	GGGGGGCAGGAGGGG [2–16]	No folding is possible
	GGGGGGGCAGGAGGG [1–15]	No folding is possible
miR-409-3p	GAAUGUUGCUCGGUG [1–15]	2xST: 1.3/2.1
miR-409-5p	GGUUACCCGAGCAAC [2–16]	2xST: −0.40/0.2
miR-429	GUCUGGUAAAACCGU [8–22]	3xST: −1.3/−1.2/−1.0
	UGUCUGGUAAAACCG [7–21]	3xST: −1.3/−1.0/−0.6
miR-432-3p	CUGGAUGGCUCCUCC [1–15]	−1.6
miR-432-5p	GAGUAGGUCAUUGGG [6–20]	1.3
	GGAGUAGGUCAUUGG [5–19]	2xST: 1.3/1.9
miR-454-3p	AUAUUGCUUAUAGGG [8–22]	4xST: 1.4/1.8/1.9/2.4
miR-454-5p	CAAUAUUGUCUCUGC [8–22]	3xST: 2.6/3.1/3.5
miR-466	ACACGCAACACACAU [9–23]	No folding is possible
	UACACGCAACACACA [8–22]	No folding is possible
	AUACACGCAACACAC [7–21]	No folding is possible
	CAUACACGCAACACA [6–20]	No folding is possible

ACAUACACGCAACAC [5–19]	No folding is possible
CACAUACACGCAACA [4–18]	No folding is possible
ACACAUACACGCAAC [3–17]	No folding is possible

[N_1–N_n]: corresponding position of the nucleotides from the circulating miRNA sequence; xST = number of possible secondary structures (predicted folding variants); [BC]: circulating miRNA also expressed in breast cancer [8]; [PC]: circulating miRNA also expressed in prostate cancer [8].

From Table 1, it can be observed that for 19 of the selected circulating miRNAs, a single aptamer sequence was predicted, while for the rest of the 17 circulating miRNAs, up to seven possible variants of sequence were predicted, with all the presented sequences having an Immunogenicity Score rank equal to 1. This suggests that the 19 miRNAs may have relatively straightforward binding requirements, and a single aptamer sequence is sufficient for specific interaction. However, for the remaining 17 circulating miRNAs, the prediction process has led to the identification of multiple possible variants of aptamer sequences. This indicates that these particular miRNAs may have more complex structural features or binding requirements that necessitate multiple candidate aptamers to achieve the desired specificity. Regardless of whether a single sequence or multiple variants were predicted, all the presented aptamer sequences have an Immunogenicity Score rank equal to 1. This implies that these aptamers are unlikely to trigger an immune response when used in practical applications, which is a favorable characteristic for diagnostic or therapeutic purposes.
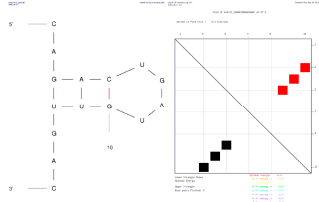
Additionally, from Table 1, it can be observed that for the 19 circulating miRNAs with only a single aptamer sequence predicted, there was also a single secondary structure variant predicted for five of them: miR-21 (negative ΔG, also expressed in breast cancer), miR-27b-3p (negative ΔG), miR-143-5p (negative ΔG, also expressed in prostate cancer), miR-218-5p (positive ΔG), and miR-432-3p (negative ΔG).

In terms of the Gibbs free energy (ΔG), utilized to predict the stability of aptamer secondary structures, it can be observed from Table 1 the following outcome:

- At least one valid secondary structure (folding variant) with negative ΔG for aptamers corresponding to 14 circulating miRNAs. Negative ΔG values suggest that these aptamers are likely to form stable secondary structures; the folding process of RNA aptamers is spontaneous and thermodynamically favored.
- At least one folding variant with positive ΔG for 19 circulating miRNAs and no folding secondary structure variants with negative ΔG. This indicates that for these miRNAs, the secondary structures of the aptamers might not be as thermodynamically stable, which could influence their binding kinetics and specificity.
- In the case of three aptamers, the folding process wasn't possible, and prediction of secondary structure failed, namely the corresponding aptamers for miR-138-1-3p (a single aptamer sequence predicted), miR-328-5p (two aptamer sequences predicted), and miR-466 (seven aptamer sequences predicted). This suggests that these particular miRNAs might pose challenges in terms of aptamer design due to their structural complexity or other factors.
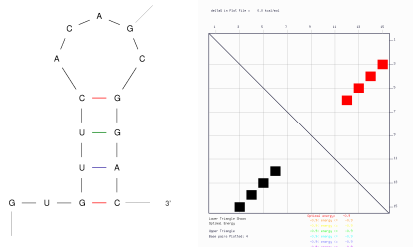
Hereinafter are presented three different case studies for folding predicted aptamer structures: (1) aptamer for miR-21 (only one predicted aptamer sequence and a single secondary structure variant with negative ΔG, Table 2), aptamers for miR-124-5p (two predicted aptamer sequences and more than one secondary structure variant, all with negative ΔG, Table 3), and miR-146a (only one predicted aptamer sequence and multiple secondary structure variants, all with positive ΔG—Table 4).
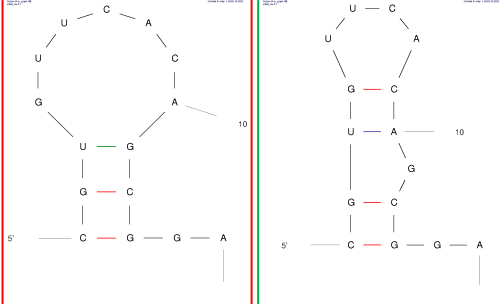
Table 2. Case study: aptamer for miR-21, predicted sequence and folding of secondary structure.

Folding of Predicted Sequence	Thermodynamics of Folding		
Sequence: CAGACUGAUGUUGAC	**Structure** $\Delta G = -0.4$ kcal/mol		
	Structural element	**δG**	**Information**
	External loop	−0.5	5 ss bases & 1 closing helix
	Stack	−1.3	External closing pair is G_3–U_{12}
	Stack	−2.2	External closing pair is A_4–U_{11}
	Helix	−3.5	3 base pairs.
	Hairpin loop	3.6	Closing pair is C_5–G_{10}

ss: single-stranded; δG values are expressed in kcal/mol.

Table 3. Case study: aptamers for miR-124-5p, predicted sequences and folding variants.

Folding of Predicted Sequence	Thermodynamics of Folding		
Sequence 1: GUGUUCACAGCGGAC	**Structure** $\Delta G = -0.9$ kcal/mol		
	Structural element	**δG**	**Information**
	External loop	0.0	2 ss bases & 1 closing helix
	Stack	−2.2	External closing pair is G_3–C_{15}
	Stack	−1.3	External closing pair is U_4–A_{14}
	Stack	−1.5	External closing pair is U_5–G_{13}
	Helix	−5.0	4 base pairs
	Hairpin loop	4.1	Closing pair is C_6–G_{12}
Sequence 2: CGUGUUCACAGCGGA	**Structure 1 (red on dot plot folding comparison)** $\Delta G = -1.1$ kcal/mol		
	Structural element	**δG**	**Information**
	External loop	−1.3	2 ss bases & 1 closing helix
	Stack	−2.4	External closing pair is C_1–G_{13}
	Stack	−2.5	External closing pair is G_2–C_{12}
	Helix	−4.9	3 base pairs
	Hairpin loop	5.1	Closing pair is U_3–G_{11}
	Structure 2 (green on dot plot folding comparison) $\Delta G = -0.5$		
	Structural element	**δG**	**Information**
	External loop	−1.3	2 ss bases & 1 closing helix
	Stack	−2.4	External closing pair is C_1–G_{13}
	Helix	−2.4	2 base pairs
	Bulge loop	1.6	External closing pair is G_2–C_{12}
	Stack	−2.1	External closing pair is U_3–A_{10}
	Helix	−2.1	2 base pairs
	Hairpin loop	3.7	Closing pair is G_4–C_9

ss: single-stranded; δG values are expressed in kcal/mol.

Table 4. Case study: aptamers for miR-146a, predicted sequences and folding variants.

Folding of Predicted Sequence	Thermodynamics of Folding		
	Structure 1 (orange on dot plot folding comparison) $\Delta G = 1.3$ kcal/mol		
Sequence: ACUGAAUUCCAUGGG	**Structural element**	**δG**	**Information**
	External loop	−1.4	9 ss bases & 1 closing helix
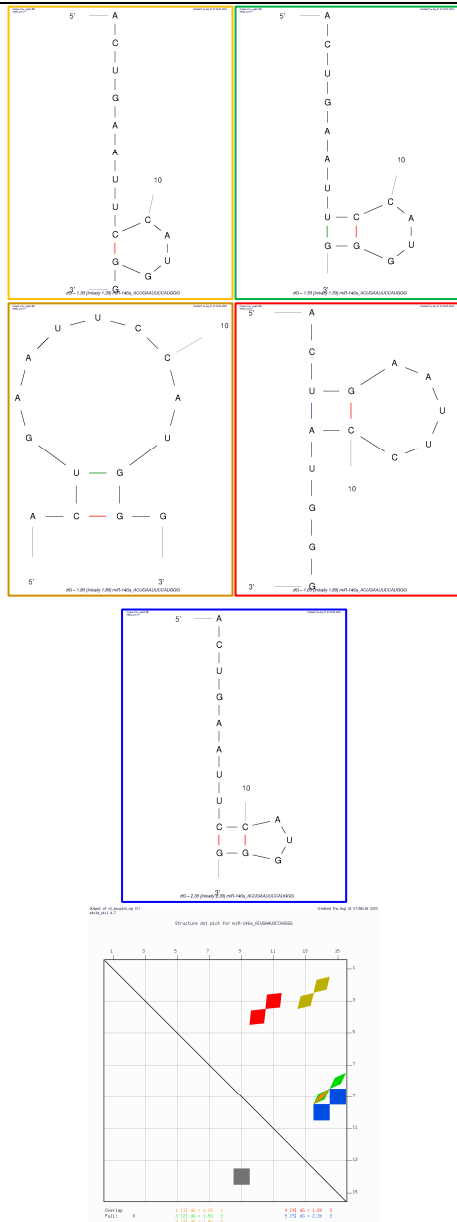
Structural element	δG	Information
Hairpin loop	2.7	Closing pair is C^9–G^{14}

Structure 2 (green on dot plot folding comparison)

ΔG = 1.5 kcal/mol

Structural element	δG	Information
External loop	0.3	7 ss bases & 1 closing helix
Stack	−1.5	External closing pair is U^8–G^{15}
Helix	−1.5	2 base pairs
Hairpin loop	2.7	Closing pair is C^9–G^{14}

Structure 3 (dark-gold on dot plot folding comparison)

ΔG = 1.8 kcal/mol

Structural element	δG	Information
External loop	−1.8	2 ss bases & 1 closing helix
Stack	−2.1	External closing pair is C^2–G^{14}
Helix	−2.1	2 base pairs
Hairpin loop	5.7	Closing pair is U^3–G^{13}

Structure 4 (red on dot plot folding comparison)

ΔG = 1.8 kcal/mol

Structural element	δG	Information
External loop	−0.2	6 ss bases & 1 closing helix
Stack	−2.1	External closing pair is U^3–A^{11}
Helix	−2.1	2 base pairs
Hairpin loop	4.1	Closing pair is G^4–C^{10}

Structure 5 (blue on dot plot folding comparison)

ΔG = 2.5 kcal/mol

Structural element	δG	Information
External loop	−0.1	8 ss bases & 1 closing helix
Stack	−3.3	External closing pair is C^9–G^{15}
Helix	−3.3	2 base pairs
Hairpin loop	5.7	Closing pair is C^{10}–G^{14}

ss: single-stranded; δG values are expressed in kcal/mol.

The miR-21 aptamer (Table 2) exhibits a single structure with a negative ΔG (−0.4 kcal/mol), indicating favorable stability and binding potential. Moreover, as a single structure was predicted for the miR-21 aptamer, the folding process is straightforward.

Two sequences were predicted for miR-124-5p (Table 3), each with a single structure variant, indicating some structural diversity but not as complex as in miR-146a (Table 4). Both miR-124-5p aptamers (Table 3) have negative ΔG values (−0.9 kcal/mol, respectively −1.1 kcal/mol), suggesting favorable folding and stability.

In contrast, all structures for the miR-146a aptamer (Table 4) have positive ΔG values, ranging from 1.3 kcal/mol to 2.5 kcal/mol, indicating unfavorable folding and instability.

Hairpin loops are significant as they often form the functional binding sites of aptamers. In all case studies, hairpin loops are present, but their thermodynamic contributions vary. For instance, they contribute positively to the stability of the miR-21 aptamers (Table 2) and miR-124-5p aptamers (Table 3) but not for the miR-146a aptamers, where positive ΔG values dominate (Table 4).

The ΔG values play a critical role in aptamer design because they reflect the stability of the interactions. Aptamers with negative ΔG values are generally preferred as they are more likely to form stable complexes with their target molecules. A negative ΔG value indicates that the aptamer-miRNA binding is thermodynamically driven and spontaneous, which is advantageous for applications such as biosensors, diagnostics, or targeted therapies. These aptamers are more likely to function effectively. The positive ΔG values indicate that these structures may struggle to form stable conformations, which could affect their binding affinity and specificity.

Accurate understanding and prediction of these values are crucial for the successful design and application of aptamers, especially in the context of cervical cancer-related miRNA detection. The structural complexity of miRNAs can pose serious challenges, and some miRNAs have intricated secondary and tertiary structures that may not be accurately captured in silico or even impossible to predict by certain computational tools in preset conditions (e.g., aptamers for miR-21, miR-124-5p, and miR-146a). This complexity can lead to difficulties in predicting ΔG values, especially if multiple conformations are possible.

It is important to note that computational predictions of ΔG values are an initial step. Experimental validation is essential to confirm the actual binding affinities and structural characteristics of these aptamers for their respective miRNA targets, especially in complex cases. Techniques such as isothermal titration calorimetry or surface plasmon resonance can provide precise ΔG measurements and confirm the binding kinetics.

4. Conclusions

In the context of cervical cancer research, these findings suggest that different circulating miRNAs may require different approaches when designing aptamers for their detection or targeting. The existence of multiple aptamer variants for some miRNAs indicates the need for careful selection and testing to determine which aptamers provide the best performance in terms of specificity and sensitivity for diagnostic or therapeutic applications related to cervical cancer.

In conclusion, the design of an innovative aptamer-based biosensor for the detection of circulating miRNAs associated with cervical cancer development holds great promise in the fight against this global health burden. By enabling early detection and personalized therapeutic interventions, this technology has the potential to improve patient outcomes and reduce the impact of cervical cancer on women's health worldwide. Continued research, validation, and collaboration are essential to realizing the full potential of this diagnostic tool and its translation into clinical practice.

Institutional Review Board Statement: Not applicable.

Informed Consent Statement: Not applicable.

Data Availability Statement: R.T is responsible for keeping and giving access to the data for the entire in silico work.

Conflicts of Interest: The author declares no conflict of interest.

References

1. Zhao, M.; Wu, Q.; Hao, Y.; Hu, J.; Gao, Y.; Zhou, S.; Han, L. Global, Regional, and National Burden of Cervical Cancer for 195 Countries and Territories, 2007–2017: Findings from the Global Burden of Disease Study 2017. *BMC Women's Health* **2021**, *21*, 419. https://doi.org/10.1186/s12905-021-01571-3.
2. Sung, H.; Ferlay, J.; Siegel, R.L.; Laversanne, M.; Soerjomataram, I.; Jemal, A.; Bray, F. Global Cancer Statistics 2020: GLOBOCAN Estimates of Incidence and Mortality Worldwide for 36 Cancers in 185 Countries. *CA A Cancer J. Clin.* **2021**, *71*, 209–249. https://doi.org/10.3322/caac.21660.

3. Zahra, Q.; Khan, Q.A.; Luo, Z. Advances in Optical Aptasensors for Early Detection and Diagnosis of Various Cancer Types. *Front. Oncol.* **2021**, *11*, 632165.
4. Sharma, A.; Dulta, K.; Nagraik, R.; Dua, K.; Singh, S.K.; Chellappan, D.K.; Kumar, D.; Shin, D.-S. Potentialities of Aptasensors in Cancer Diagnosis. *Mater. Lett.* **2022**, *308*, 131240. https://doi.org/10.1016/j.matlet.2021.131240.
5. Kher, G.; Trehan, S.; Misra, A. Antisense Oligonucleotides and RNA Interference. In *Challenges in Delivery of Therapeutic Genomics and Proteomics*; Misra, A., Ed.; Elsevier: London, UK, 2011; pp. 325–386, ISBN 978-0-12-384964-9.
6. Abbas, M.; Mehdi, A.; Khan, F.H.; Verma, S.; Ahmad, A.; Khatoon, F.; Raza, S.T.; Afreen, S.; Glynn, S.A.; Mahdi, F. Role of MiRNAs in Cervical Cancer: A Comprehensive Novel Approach from Pathogenesis to Therapy. *J. Gynecol. Obstet. Hum. Reprod.* **2021**, *50*, 102159. https://doi.org/10.1016/j.jogoh.2021.102159.
7. Doghish, A.S.; Ali, M.A.; Elyan, S.S.; Elrebehy, M.A.; Mohamed, H.H.; Mansour, R.M.; Elgohary, A.; Ghanem, A.; Faraag, A.H.I.; Abdelmaksoud, N.M.; et al. MiRNAs Role in Cervical Cancer Pathogenesis and Targeted Therapy: Signaling Pathways Interplay. *Pathol.—Res. Pract.* **2023**, *244*, 154386. https://doi.org/10.1016/j.prp.2023.154386.
8. Galvão-Lima, L.J.; Morais, A.H.F.; Valentim, R.A.M.; Barreto, E.J.S.S. MiRNAs as Biomarkers for Early Cancer Detection and Their Application in the Development of New Diagnostic Tools. *BioMedical Eng. OnLine* **2021**, *20*, 21. https://doi.org/10.1186/s12938-021-00857-9.
9. RNAcentral Consortium. RNAcentral 2021: Secondary Structure Integration, Improved Sequence Search and New Member Databases. *Nucleic Acids Res.* **2021**, *49*, D212–D220. https://doi.org/10.1093/nar/gkaa921.
10. Pisitkun, T.; Hoffert, J.D.; Saeed, F.; Knepper, M.A. NHLBI-AbDesigner: An Online Tool for Design of Peptide-Directed Antibodies. *Am. J. Physiol. Cell Physiol.* **2012**, *302*, C154–C164. https://doi.org/10.1152/ajpcell.00325.2011.
11. Zuker, M. Mfold Web Server for Nucleic Acid Folding and Hybridization Prediction. *Nucleic Acids Res.* **2003**, *31*, 3406–3415.
12. Zuber, J.; Schroeder, S.J.; Sun, H.; Turner, D.H.; Mathews, D.H. Nearest Neighbor Rules for RNA Helix Folding Thermodynamics: Improved End Effects. *Nucleic Acids Res.* **2022**, *50*, 5251–5262. https://doi.org/10.1093/nar/gkac261.